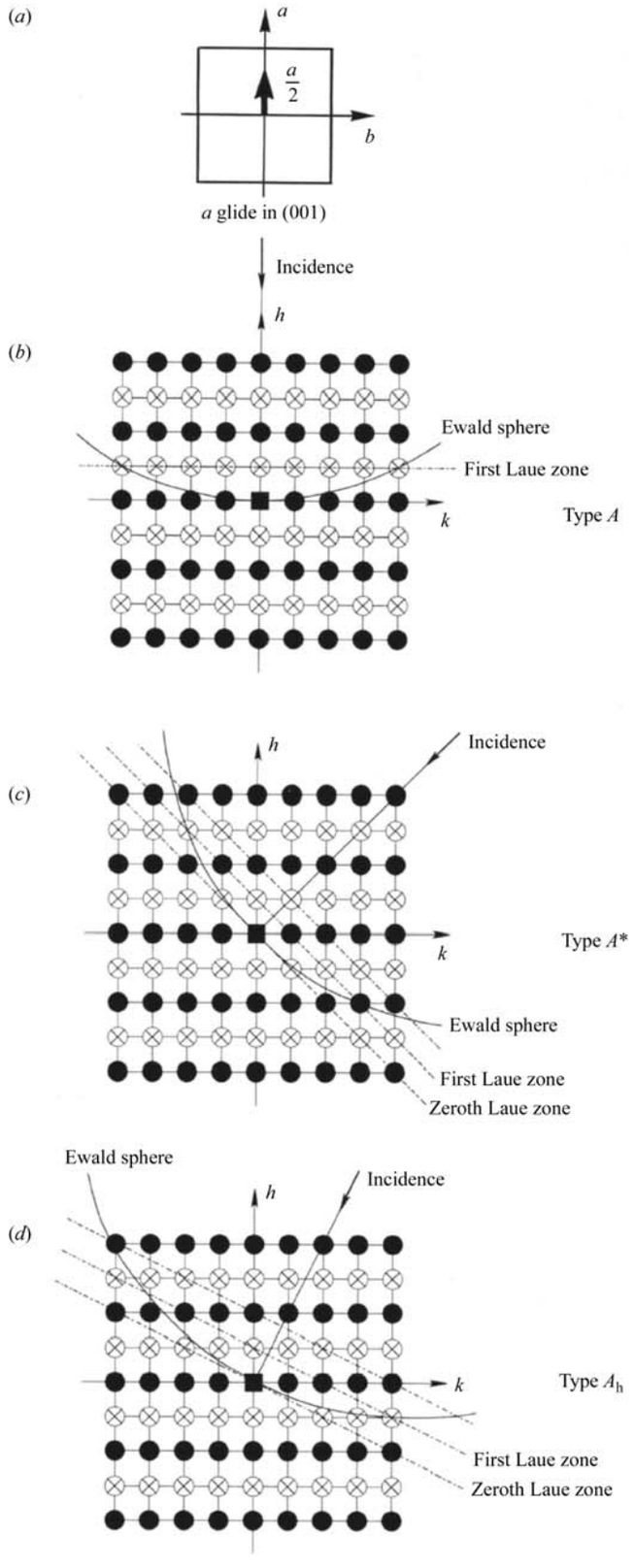

Fig. 2.5.3.13. Illustration of dynamical extinction lines appearing in HOLZ reflections due to glide planes. Black circles and circled crosses show kinematically allowed and kinematically forbidden reflections, respectively. (*a*) *a* glide in the (001) plane. (*b*) [100] incidence: dynamical extinction lines are formed in HOLZ reflections on both sides of the incident beam (type *A*). (*c*) [110] incidence: an extinction line is formed at a HOLZ reflection on one side of the incident beam because on the other side the Ewald sphere intersects an allowed HOLZ reflection (type *A**). (*d*) An incidence between [100] and [110]: an extinction line is formed at a HOLZ reflection on one side of the incident beam because on the other side the Ewald sphere does not intersect a HOLZ reflection (type A_h).

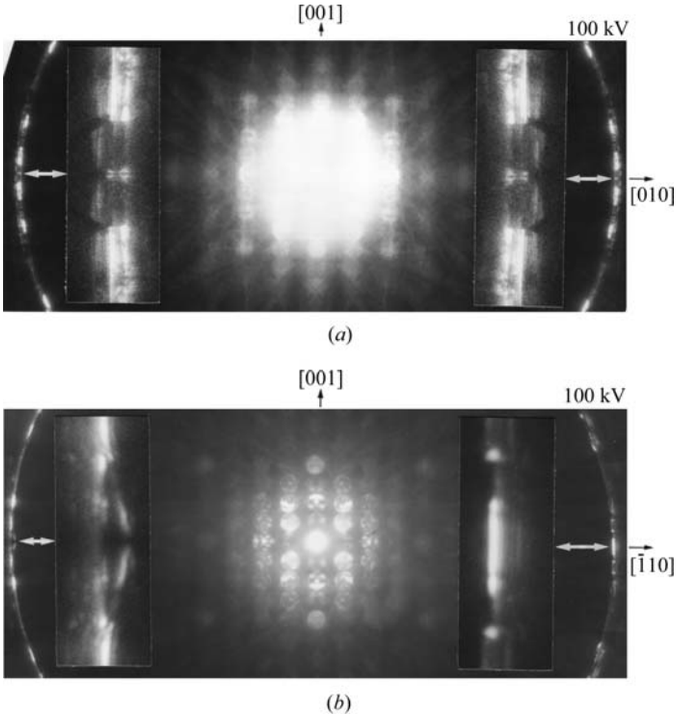

Fig. 2.5.3.14. HOLZ CBED pattern of FeS_2. (*a*) [100] incidence: type *A* dynamical extinction lines are seen clearly in the enlarged insets. (*b*) [110] incidence: a type *A** dynamical extinction line is seen clearly in the enlarged insets.

which satisfies the results obtained at the two crystal orientations is $\bar{4}3m$.

Fig. 2.5.3.16(*e*) shows an ordinary diffraction pattern taken with the [100] incidence at 80 kV. With the help of the lattice parameters and the camera length, the indices of the reflections are given as shown in the figure. The reflections $0kl$ ($k + l = 2n + 1$) are found to be kinematically forbidden. Thus, the lattice type is determined to be *I*.

The space groups having point group $\bar{4}3m$ and lattice type *I* are $I\bar{4}3m$ and $I\bar{4}3d$ from Table 2.5.3.9. Fig. 2.5.3.16(*d*) shows dynamical extinction lines A_2 in the 033 disc and equivalent discs (also broad lines A_2 in the 011 discs). Since the former space group does not give any dynamical extinction lines, the space group is determined to be $I\bar{4}3d$. For confirmation, a CBED pattern which contains the second-order-Laue-zone reflections was taken (Fig. 2.5.3.16*f*). Dynamical extinction lines *A* are seen in the 2,22,22 disc and the equivalent discs. This result also identifies the space group to be not $I\bar{4}3m$ but $I\bar{4}3d$ with the aid of Table 2.5.3.12.

2.5.3.4. Symmetry determination of incommensurate crystals

2.5.3.4.1. General remarks

Incommensurately modulated crystals do not have three-dimensional lattice periodicity. The crystals, however, recover lattice periodicity in a space higher than three dimensions. de Wolff (1974, 1977) showed that one-dimensional displacive and substitutionally modulated crystals can be described as a three-dimensional section of a (3 + 1)-dimensional periodic crystal. Janner & Janssen (1980*a*,*b*) developed a more general approach for describing a modulated crystal with *n* modulations as (3 + *n*)-dimensional periodic crystals ($n = 1, 2, \ldots$). Yamamoto (1982) derived a general structure-factor formula for *n*-dimensionally modulated crystals ($n = 1, 2, \ldots$), which holds for both displacive and substitutionally modulated crystals. Tables of the (3 + 1)-dimensional space groups for one-dimensional incommensurately modulated crystals were given by de Wolff *et al.* (1981), where the wavevector of the modulation was assumed to lie in the

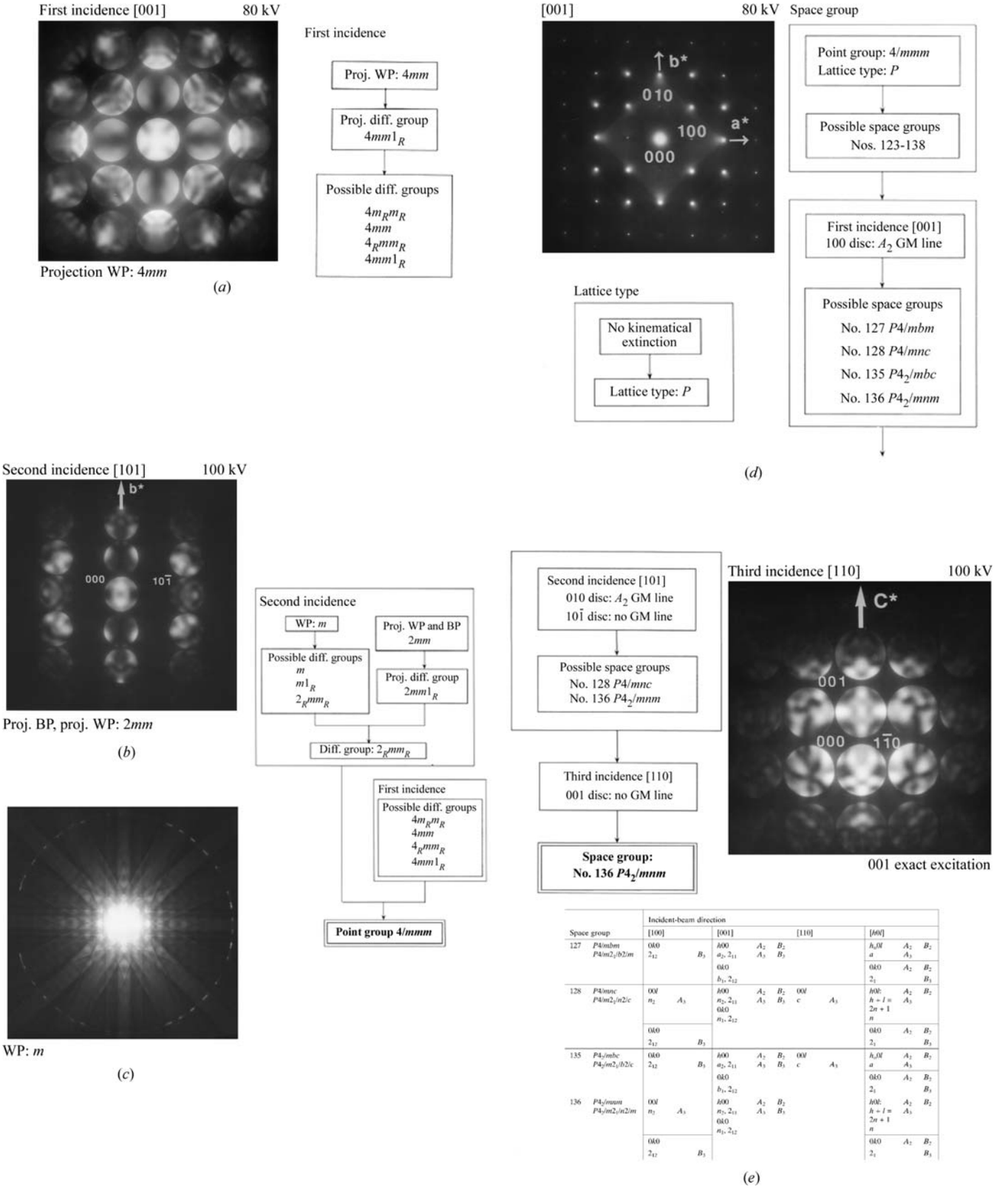

Space group		Incident-beam direction [100]		[001]				[110]			[h0l]		
127	P4/mbm P4/m2$_1$/b2/m	0k0 2_{12}	B_3	h00 $a_2, 2_{11}$ 0k0 $b_1, 2_{12}$	A_2 A_3	B_2 B_3				h_n0l a 0k0 2_1	A_2 A_3 A_2	B_2 B_3 B_2 B_3
128	P4/mnc P4/m2$_1$/n2/c	00l n_2	A_3	h00 $n_2, 2_{11}$ 0k0 $n_1, 2_{12}$	A_2 A_3	B_2 B_3	00l c	A_3		h0l: $h + l =$ $2n + 1$ n	A_2 A_3	B_2
		0k0 2_{12}	B_3							0k0 2_1	A_2	B_2 B_3
135	P4$_2$/mbc P4$_2$/m2$_1$/b2/c	0k0 2_{12}	B_3	h00 $a_2, 2_{11}$ 0k0 $b_1, 2_{12}$	A_2 A_3	B_2 B_3	00l c	A_3		h_n0l a 0k0 2_1	A_3 A_3 A_2	B_2 B_3 B_2 B_3
136	P4$_2$/mnm P4$_2$/m2$_1$/n2/m	00l n_2	A_3	h00 $n_2, 2_{11}$ 0k0 $n_1, 2_{12}$	A_2 A_3	B_2 B_3				h0l: $h + l =$ $2n + 1$ n	A_2 A_3	B_2
		0k0 2_{12}	B_3							0k0 2_1	A_2	B_2 B_3

Fig. 2.5.3.15. CBED patterns of rutile. The procedures for identifying the symmetry are also shown. (*a*) [001] incidence at 80 kV: the projection (proj.) WP shows symmetry 4*mm*. (*b*, *c*) [101] incidence at 100 kV: the projection BP and projection WP show symmetry 2*mm* and the WP shows symmetry *m* (the point group is 4/*mmm*). (*d*) Spot diffraction pattern showing no extinction caused by the lattice type (lattice type *P*). (*e*) Near-[110] incidence at 100 kV to excite exactly the 001 reflection: no extinction lines in the 001 disc (space group $P4_2/mnm$).

c direction. Later, some corrections to the tables were made by Yamamoto *et al.* (1985). The analysis of incommensurately modulated crystals using (3 + 1)-dimensional space groups has become familiar in the field of X-ray structure analysis.

Fung *et al.* (1980) applied the CBED method to the study of incommensurately modulated transition-metal dichalcogenides. Steeds *et al.* (1985) applied the LACBED method (Tanaka *et al.*, 1980) to the study of incommensurately modulated crystals of $NiGe_{1-x}P_x$. Tanaka *et al.* (1988, pp. 74–81) examined the symmetries of the incommensurate and fundamental reflections appearing in the CBED patterns obtained from the incommensurately modulated crystals of $Sr_2Nb_2O_7$ and Mo_8O_{23}. Terauchi &

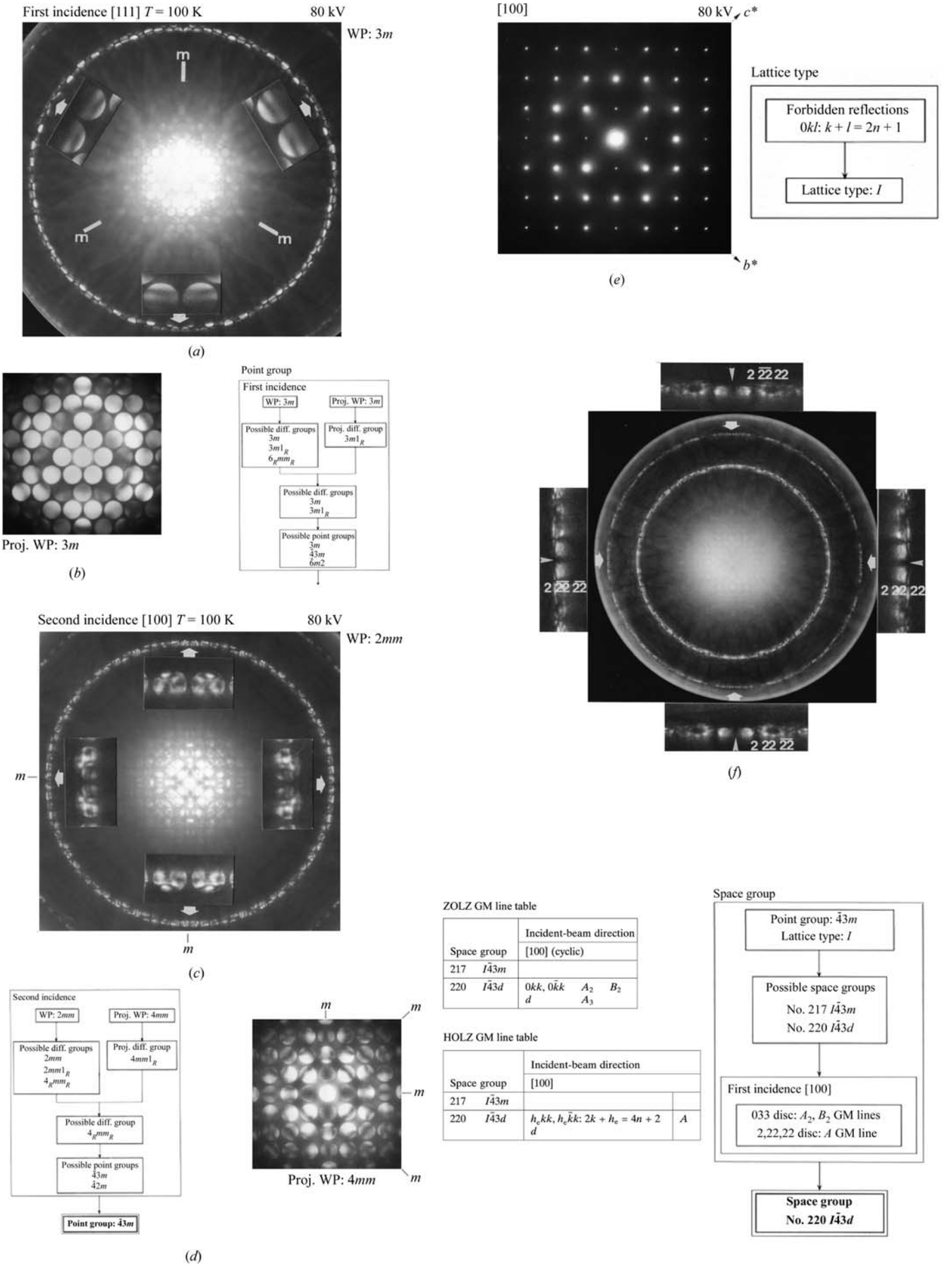

Fig. 2.5.3.16. CBED patterns of Sm_3Se_4. The procedures for identifying the symmetry are also shown. (*a*, *b*) [111] incidence at 80 kV: the WP symmetry is 3*m* (*a*) and the projection (proj.) WP symmetry is 3*m* (*b*). (*c*, *d*) [100] incidence at 80 kV: the WP symmetry is 2*mm* (*c*) and the projection WP symmetry is 4*mm* (*d*). Dynamical extinction lines A_2 and A_3 are seen (*d*). The point group is determined to be $\bar{4}3m$. (*e*) Spot diffraction pattern taken with the [100] incidence at 80 kV shows the absence of 0*kl* reflections. The lattice type is determined to be *I*. (*f*) [100] incidence at 100 kV: dynamical extinction lines *A* in HOLZ reflections confirm the existence of a glide plane. The space group is determined to be $I\bar{4}3d$.

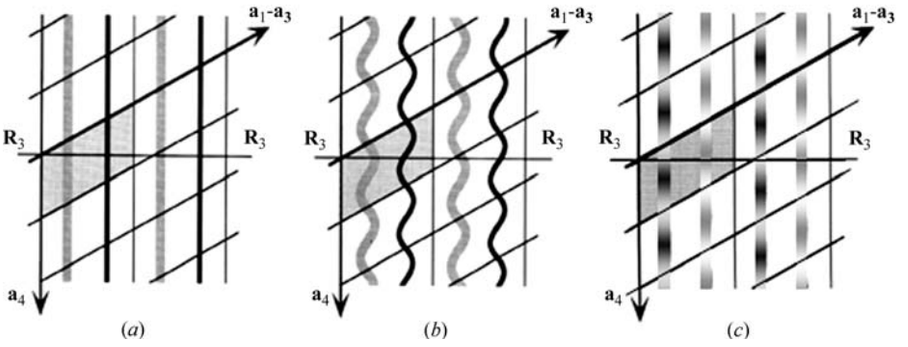

Fig. 2.5.3.17. The (3 + 1)-dimensional description of one-dimensionally modulated crystals. Atoms are shown as strings along the fourth direction $\mathbf{a}_4$. (*a*) No modulation, shown as straight strings. (*b*) Displacive modulation, shown as wavy strings. (*c*) Amplitude modulation with varying-density strings.

Tanaka (1993) clarified theoretically the interrelation between the symmetries of CBED patterns and the (3 + 1)-dimensional point-group symbols for incommensurately modulated crystals and verified experimentally the theoretical results for $Sr_2Nb_2O_7$ and Mo_8O_{23}. Terauchi *et al.* (1994) investigated dynamical extinction for the (3 + 1)-dimensional space groups. They clarified that approximate dynamical extinction lines appear in CBED discs of the reflections caused by incommensurate modulations when the amplitudes of the incommensurate modulation waves are small. They tabulated the dynamical extinction lines appearing in the CBED discs for all the (3 + 1)-dimensional space groups of the incommensurately modulated crystals. The tables were stored in the British Library Document Supply Centre as Supplementary Publication No. SUP 71810 (65 pp.). They showed an example of the dynamical extinction lines obtained from $Sr_2Nb_2O_7$. The point- and space-group determinations of the (3 + 1)-dimensional crystals are described compactly in the book by Tanaka *et al.* (1994, pp. 156–205).

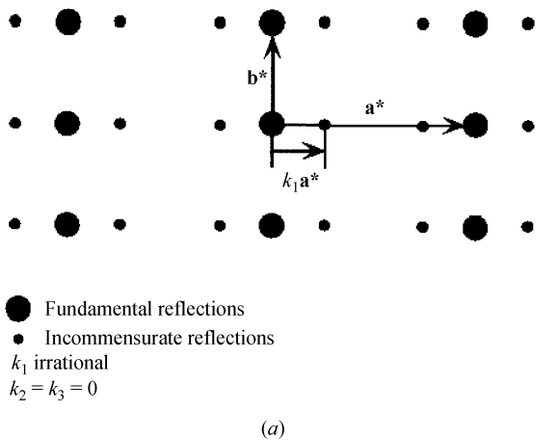

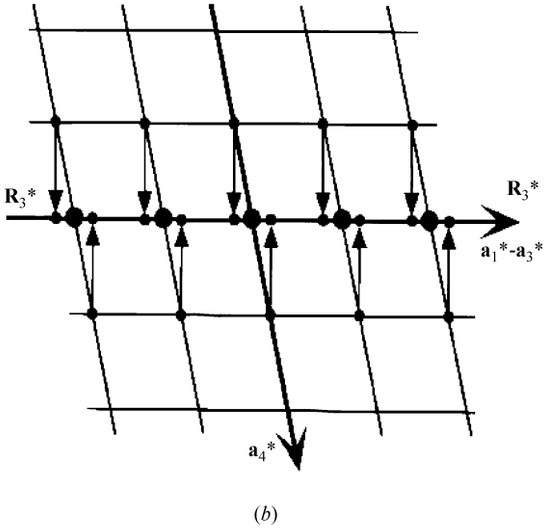

Fig. 2.5.3.18. (*a*) Schematic diffraction pattern from a modulated crystal. As an example, the wave number vector of modulation is assumed to be $k_1\mathbf{a}^*$, k_1 being an irrational number. Large and small spots denote fundamental and incommensurate reflections, respectively. (*b*) Incommensurate reflections are obtained by a projection of the Fourier transform of a (3 + 1)-dimensional periodic structure.

Fig. 2.5.3.17 illustrates (3 + 1)-dimensional descriptions of a crystal structure without modulation (*a*), a one-dimensional displacive modulated structure (*b*) and a one-dimensional substitutionally modulated structure (*c*). The arrows labelled $\mathbf{a}_1$–$\mathbf{a}_3$ (**a**, **b** and **c**) and $\mathbf{a}_4$ indicate the (3 + 1)-dimensional crystal axes. The horizontal line labelled $\mathbf{R}_3$ represents the three-dimensional space (external space). In the (3 + 1)-dimensional description, an atom is not located at a point as in the three-dimensional space, but extends as a string along the fourth direction $\mathbf{a}_4$ perpendicular to the three-dimensional space $\mathbf{R}_3$. The shaded parallelogram is a unit cell in the (3 + 1)-dimensional space. The unit cell contains two atom strings in this case. In the case of no modulations, the atoms are shown as straight strings, as shown in Fig. 2.5.3.17(*a*). For a displacive modulation, atoms are expressed by wavy strings periodic along the fourth direction $\mathbf{a}_4$ as shown in Fig. 2.5.3.17(*b*). The width of the atom strings indicates the spread of the atoms in $\mathbf{R}_3$. The atom positions of the modulated structure in $\mathbf{R}_3$ are given as a three-dimensional ($\mathbf{R}_3$) section of the atom strings in the (3 + 1)-dimensional space. A substitutional modulation, which is described by a modulation of the atom form factor, is expressed by atom strings with a density modulation along the direction $\mathbf{a}_4$ as shown in Fig. 2.5.3.17(*c*).

The diffraction vector **G** is written as

$$\mathbf{G} = h_1\mathbf{a}^* + h_2\mathbf{b}^* + h_3\mathbf{c}^* + h_4\mathbf{k},$$

where a set of $h_1h_2h_3h_4$ is a (3 + 1)-dimensional reflection index, and **a***, **b*** and **c*** are the reciprocal-lattice vectors of the real-lattice vectors **a**, **b** and **c** of the average structure. The modulation vector **k** is written as

$$\mathbf{k} = k_1\mathbf{a}^* + k_2\mathbf{b}^* + k_3\mathbf{c}^*,$$

where one coefficient k_i (i = 1–3) is an irrational number and the others are rational. Fig. 2.5.3.18(*a*) shows a diffraction pattern of a crystal with an incommensurate modulation wavevector $k_1\mathbf{a}^*$ (k_2 and k_3 = 0). Large and small black spots show the fundamental reflections and incommensurate reflections, respectively, only the first-order incommensurate reflections being shown. It

should be noted that the diffraction pattern of a modulated crystal is obtained by a projection of the Fourier transform of the (3 + 1)-dimensional periodic structure. Fig. 2.5.3.18(*b*) is assumed to be the Fourier transform of Fig. 2.5.3.17(*b*). Incommensurate reflections are obtained by a projection of the reciprocal-lattice points onto $\mathbf{R}_3^*$.

The displacive modulation is expressed by the atom displacement u_i^μ with x_4. The structure factor $F(h_1h_2h_3h_4)$ for the (3 + 1)-dimensional crystal with a displacive modulation is given by de Wolff (1974, 1977) as follows:

$$F(h_1h_2h_3h_4) = \sum_{\mu=1}^{N} f_\mu \exp[2\pi i(h_1\bar{x}_1^\mu + h_2\bar{x}_2^\mu + h_3\bar{x}_3^\mu)] \times \int_0^1 \exp\left\{2\pi i\left[\sum_{i=1}^{3}(h_i + h_4k_i)u_i^\mu + h_4\bar{x}_4^\mu\right]\right\} \mathrm{d}\bar{x}_4^\mu, \tag{2.5.3.6}$$

where

$$\bar{x}_4^\mu = (\bar{x}_1^\mu + n_1)k_1 + (\bar{x}_2^\mu + n_2)k_2 + (\bar{x}_3^\mu + n_3)k_3.$$

f_μ and $\bar{x}_i^\mu (i = 1\text{–}3)$ are, respectively, the atom form factor and the ith component of the position of the μth atom in the unit cell of the average structure. The symbol u_i^μ is the ith component of the displacement of the μth atom. Since the atom in the (3 + 1)-dimensional space is continuous along $\mathbf{a}_4$ and discrete along $\mathbf{R}_3$, the structure factor is expressed by summation in $\mathbf{R}_3$ and integration along $\mathbf{a}_4$ as seen in equation (2.5.3.6). The integration implies that the sum for the atoms with displacements is taken over the infinite number of unit cells of the average structure. That is, equation (2.5.3.6) is the structure factor for a unit cell with the lattice parameter of an infinite length in $\mathbf{R}_3$ along the direction of the modulation wavevector $\mathbf{k}$.

CBED patterns are obtained from a finite area of a specimen crystal. For the symmetry analysis of CBED patterns obtained from modulated structures, the effect of the finite size was considered by Terauchi & Tanaka (1993). The integration over a unit-cell length along $\mathbf{a}_4$ in equation (2.5.3.6) is rewritten in the following way with the summation over a finite number of three-dimensional sections of the atom strings:

$$F'(h_1h_2h_3h_4) = \sum_{\mu=1}^{N} f_\mu \exp[2\pi i(h_1\bar{x}_1^\mu + h_2\bar{x}_2^\mu + h_3\bar{x}_3^\mu)] \times \sum_{n_1}\sum_{n_2}\sum_{n_3} \exp\left\{2\pi i\left[\sum_{i=1}^{3}(h_i + h_4k_i)u_i^\mu + h_4\bar{x}_4^\mu\right]\right\}, \tag{2.5.3.7}$$

where $N_1 < n_1 \le N_1'$, $N_2 < n_2 \le N_2'$ and $N_3 < n_3 \le N_3'$, $N' = (N_1' - N_1)(N_2' - N_2)(N_3' - N_3)$ being the number of unit cells of the average structure included in a specimen volume from which CBED patterns are taken.

The substitutional modulation arises from a periodic variation of the site-occupation probability of the atoms. This modulation is expressed by a modulation of the atom form factor f_μ with x_4. The structure factor $F'(h_1h_2h_3h_4)$ for a finite-size crystal is written as

$$F'(h_1h_2h_3h_4) = \sum_{\mu=1}^{N} \exp[2\pi i\,(h_1x_1^\mu + h_2x_2^\mu + h_3x_3^\mu)] \times \sum_{n_1}\sum_{n_2}\sum_{n_3} f_\mu \exp(2\pi i h_4 x_4^\mu), \tag{2.5.3.8}$$

where $x_4^\mu = \sum_i (x_i^\mu + n_i)k_i$.

2.5.3.4.2. Point-group determination

The symmetries of the CBED patterns can be determined by examination of the symmetries of the structure factor $F'(h_1h_2h_3h_4)$ in equations (2.5.3.7) or (2.5.3.8). We consider a displacive modulated structure, which has a modulation wavevector $\mathbf{k} = k_3\mathbf{c}^*$ and belongs to (3 + 1)-dimensional space group $P^{P2/m}_{1\ \bar{1}}$. This space-group symbol implies the following.

(1) The modulation wavevector $\mathbf{k}$ exists inside the first Brillouin zone of the average structure (P).

(2) The average structure belongs to space group $P2/m$, the twofold rotation axis being parallel to the c axis.

(3) The symmetry subsymbol 1, which is written beneath symmetry symbol 2, indicates that the modulation wavevector $\mathbf{k}$ is transformed into itself by symmetry operation 2 of the average structure. The symmetry subsymbol beneath symmetry symbol m indicates that the wavevector $\mathbf{k}$ is transformed into $-\mathbf{k}$ by symmetry operation m. The modulated structure has a twofold rotation axis, which is common to the average structure, but does not have mirror symmetry, which is possessed by the average structure.

For the twofold rotation axis (symbol 2) of this space group, the structure factor $F'(h_1h_2h_3h_4)$ is written as

$$\begin{aligned} F'(h_1h_2h_3h_4) &= \sum_{\mu=1}^{N} f_\mu \exp[2\pi i(h_1\bar{x}_1^\mu + h_2\bar{x}_2^\mu + h_3\bar{x}_3^\mu)] \\ &\quad \times \sum_{n_3} \exp\{2\pi i[h_1u_1^\mu + h_2u_2^\mu + (h_3 + h_4k_3)u_3^\mu + h_4\bar{x}_4^\mu]\} \\ &\quad + \sum_{\mu=1}^{N} f_\mu \exp[2\pi i(-h_1\bar{x}_1^\mu - h_2\bar{x}_2^\mu + h_3\bar{x}_3^\mu)] \\ &\quad \times \sum_{n_3} \exp\{2\pi i[-h_1u_1^\mu - h_2u_2^\mu + (h_3 + h_4k_3)u_3^\mu + h_4\bar{x}_4^\mu]\}, \end{aligned} \tag{2.5.3.9}$$

where $x_4^\mu = (x_3^\mu + n_3)k_3$. It is found from equation (2.5.3.9) that two structure factors $F'(h_1h_2h_3h_4)$ and $F'(\bar{h}_1\bar{h}_2h_3h_4)$ are the same when reflections $h_1h_2h_3h_4$ and $\bar{h}_1\bar{h}_2h_3h_4$ are equivalent with respect to the twofold rotation axis of the average structure. Thus, not only fundamental reflections ($h_4 = 0$) from the average structure but also the satellite reflections ($h_4 \neq 0$) from the incommensurate structure show twofold rotation symmetry about the c^* axis.

For the mirror plane (symbol m), the structure factor is written in a similar manner to the case of the twofold rotation axis. It is found that $F'(h_1h_2h_3h_4)$ is not equal to $F'(h_1h_2\bar{h}_3\bar{h}_4)$ for the incommensurate reflections $h_4 \neq 0$. Hence, the incommensurate reflections do not show mirror symmetry with respect to the mirror plane of the average structure. For the fundamental reflections ($h_4 = 0$), $F'(h_1h_2h_3h_4)$ is equal to $F'(h_1h_2\bar{h}_3\bar{h}_4)$, indicating the existence of mirror symmetry. It should be noted that the mirror symmetry can be destroyed by the dynamical diffraction effect between the fundamental and incommensurate reflections. In most modulated structures, however, the amplitude of the modulation wave u_i^μ is not so large as to destroy the symmetry of the fundamental reflections. Thus, the fundamental

Table 2.5.3.13. *Wavevectors, point- and space-group symbols and CBED symmetries of one-dimensionally modulated crystals*

Wavevector transformation	Point-group symbol	Symmetry of incommensurate reflection	Space-group symbol	Dynamical extinction lines
$\mathbf{k} \rightarrow \mathbf{k}$	1	Same symmetry as average structure	1, s (1/2), t ($\pm$1/3), q ($\pm$1/4), h ($\pm$1/6)	Yes for s, q and h
$\mathbf{k} \rightarrow -\mathbf{k}$	$\bar{1}$	No symmetry	$\bar{1}$	No

reflections ought to show the symmetry of the average structure, while the incommensurate reflections lose the symmetry.

The problem of the finite size of the illuminated area is discussed using equations (2.5.3.7) and (2.5.3.8) in a paper by Terauchi & Tanaka (1993) and in the book by Tanaka *et al.* (1994, pp. 156–205). The results are as follows: Even if the size and position of an illuminated specimen area are changed, the intensity distribution in a CBED pattern changes but the symmetry of the pattern does not. To obtain the symmetries of incommensurate crystals, it is not necessary to take CBED patterns from an area whose diameter is larger than the period of the modulated structure. The symmetries of the modulated structure can appear when more than one unit cell of the average structure is illuminated for displacive modulations. For substitutional modulations, a specimen volume that produces the average atom form factor is needed, namely a volume of about 1 nm diameter area and 50 nm thick.

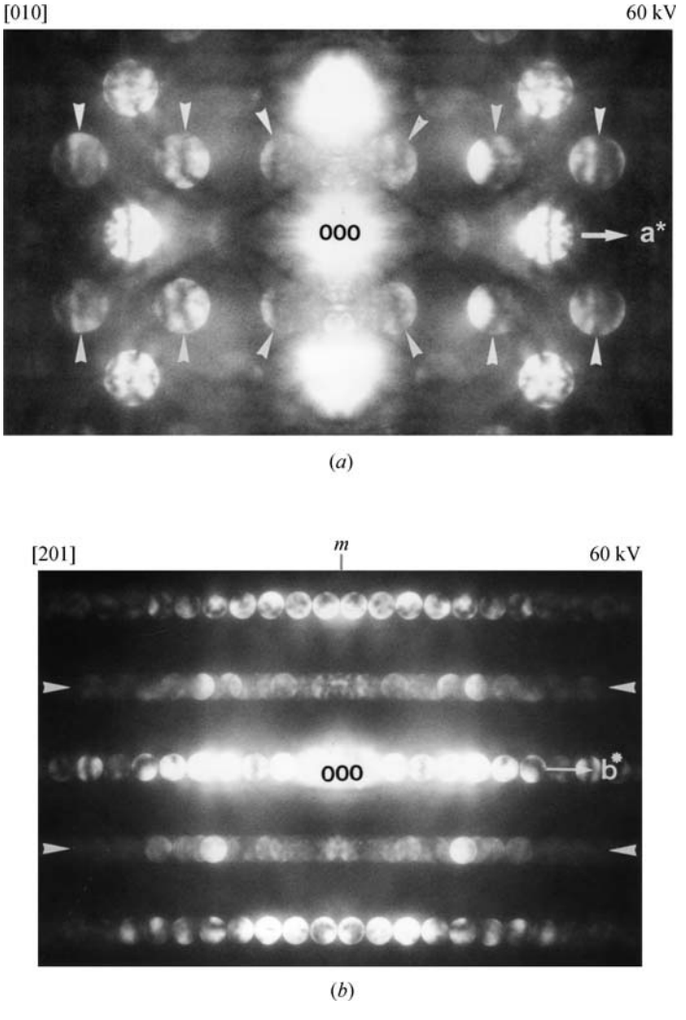

Fig. 2.5.3.19. CBED patterns of the incommensurate phase of $Sr_2Nb_2O_7$ taken at 60 kV. (*a*) [010] incidence: fundamental reflections show a mirror symmetry perpendicular to the a^* axis but incommensurate reflections do not [symmetry ($^m_1$)]. (*b*) [201] incidence: incommensurate reflections show mirror symmetry perpendicular to the b^* axis [symmetry ($^m_1$)]. The wave number vector of the modulation is $\mathbf{k} = (\frac{1}{2} - \delta)\mathbf{a}^*$.

Table 2.5.3.13 shows the point-group symmetries (third column) of the incommensurate reflections for the two point-group subsymbols. For symmetry subsymbol 1, both the fundamental and incommensurate reflections show the symmetries of the average structure. For symmetry subsymbol $\bar{1}$, the fundamental reflections show the symmetries of the average structure but the incommensurate reflections do not have any symmetry. These facts imply that the symmetries of the incommensurate reflections are determined by the point group of the average structure and the modulation wavevector **k**. In other words, observation of the symmetries of the incommensurate reflections is not necessary for the determination of the point groups, although it can ascertain the point groups of the modulated crystals.

An example of point-group determination is shown for the incommensurate phase of $Sr_2Nb_2O_7$. Many materials of the $A_2B_2O_7$ family undergo phase transformations from space group $Cmcm$ to $Cmc2_1$ and further to $P2_1$ with decreasing temperature. An incommensurate phase appears between the $Cmc2_1$ phase and the $P2_1$ phase. $Sr_2Nb_2O_7$ transforms at 488 K from the $Cmc2_1$ phase into the incommensurate phase with a modulation wavevector $\mathbf{k} = (\frac{1}{2} - \delta)\mathbf{a}^*$ (δ = 0.009–0.023) but does not transform into the $P2_1$ phase. The space group of $Sr_2Nb_2O_7$ was reported as $P^{C\,mc2_1}_{\bar{1}s\bar{1}}$ (Yamamoto, 1988). (Since the space-group notation $Cmc2_1$ is broadly accepted, the direction of the modulation is taken as the a axis.) The point group of the phase is $^{mm2}_{\bar{1}\,\bar{1}\,1}$. The modulation wavevector **k** is transformed to $-\mathbf{k}$ by the mirror symmetry operation perpendicular to the a axis ($^m_1$) and by the twofold rotation symmetry operation about the c axis ($^2_1$). The wavevector is transformed into itself by the mirror symmetry operation perpendicular to the b axis ($^m_1$).

Fig. 2.5.3.19(*a*) shows a CBED pattern of the incommensurate phase of $Sr_2Nb_2O_7$ taken with the [010] incidence at an accelerating voltage of 60 kV. The reflections indicated by arrowheads are the incommensurate reflections. Other reflections are the fundamental reflections. Since the pattern is produced by the interaction of the reflections in the zeroth-order Laue zone, symmetry operations ($^m_1$) and ($^2_1$) act the same. These symmetries are confirmed by the fact that the fundamental reflections show mirror symmetry perpendicular to the a^* axis (twofold rotation symmetry about the c^* axis) but the incommensurate reflections do not. Fig. 2.5.3.19(*b*) shows a CBED pattern of the incommensurate phase of $Sr_2Nb_2O_7$ taken with the [201] incidence at 60 kV. The reflections in the two rows indicated by arrowheads are the incommensurate reflections and the others are the fundamental reflections. Symmetry symbol ($^m_1$) implies that both the fundamental and incommensurate reflections display mirror symmetry perpendicular to the b^* axis. Fig. 2.5.3.19(*b*) exactly exhibits the symmetry.

2.5.3.4.3. Space-group determination

Table 2.5.3.13 shows the space-group symbols (fourth column) of the modulated crystals. When a glide (screw) component τ_4 between the modulation waves of two atom rows is 0, 1/2, $\pm$1/3, $\pm$1/4 or $\pm$1/6, symbol 1, s, t, q or h is given, respectively (de Wolff *et al.*, 1981). Such glide components are allowed for point-group symmetry 1 but are not for point-group symmetry $\bar{1}$. Dynamical

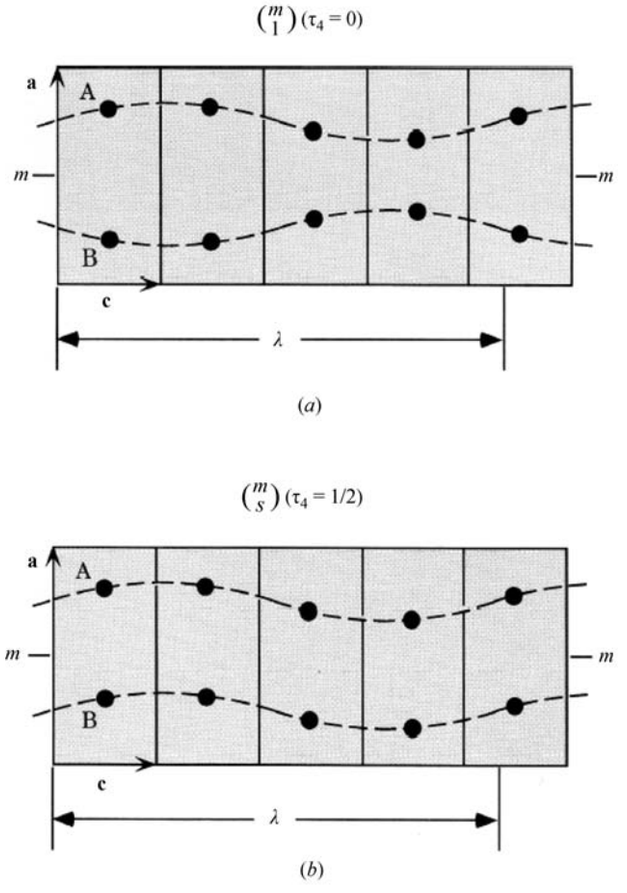

Fig. 2.5.3.20. (*a*) Mirror symmetry of modulation waves $\binom{m}{1}$ $\tau_4 = 0$. (*b*) Glide symmetry of modulation waves $\binom{m}{s}$ $\tau_4 = \frac{1}{2}$. The wave number vector of modulation is $k_3\mathbf{c}^*$.

extinction occurs for glide components *s*, *q* and *h* but does not for glide component *t*. When the average structure does not have a glide component, dynamical extinction due to a glide component τ_4 appears in odd-order incommensurate reflections. When the average structure has a glide component, dynamical extinction due to a glide component τ_4 appears in incommensurate reflections with $h_i + h_4 = 2n + 1$, where h_i and h_4 are the reflection indices for the average structure and incommensurate structure, respectively. Details are given in the paper by Terauchi *et al.* (1994).

Fig. 2.5.3.20(*a*) illustrates mirror symmetry $\binom{m}{1}$ between atom rows A and B, which is perpendicular to the *b* axis with no glide component ($\tau_4 = 0$). Here, the wave number vector of the modulation is assumed to be $\mathbf{k} = k_3\mathbf{c}^*$ following the treatment of de Wolff *et al.* (1981). Fig. 2.5.3.20(*b*) illustrates glide symmetry $\binom{m}{s}$ with a glide component $\tau_4 = \frac{1}{2}$. The structure factor $F(h_1h_2h_3h_4)$ is written for the glide plane $\binom{m}{s}$ of an infinite incommensurate crystal as

$$\begin{aligned}
&F(h_1h_2h_3h_4)\\
&= \sum_{\mu=1}^{N} f_\mu \exp[2\pi i(h_1\bar{x}_1^\mu + h_2\bar{x}_2^\mu + h_3\bar{x}_3^\mu)]\\
&\quad \times \int_0^1 \exp\{2\pi i[h_1u_1^\mu + h_2u_2^\mu + (h_3 + h_4k_3)u_3^\mu + h_4\bar{x}_4^\mu]\}\,\mathrm{d}\bar{x}_4^\mu\\
&\quad + \exp(h_4\pi i)\sum_{\mu=1}^{N} f_\mu \exp[2\pi i(h_1\bar{x}_1^\mu - h_2\bar{x}_2^\mu + h_3\bar{x}_3^\mu)]\\
&\quad \times \int_0^1 \exp\{2\pi i[h_1u_1^\mu - h_2u_2^\mu + (h_3 + h_4k_3)u_3^\mu + h_4\bar{x}_4^\mu]\}\,\mathrm{d}\bar{x}_4^\mu.
\end{aligned} \tag{2.5.3.10}$$

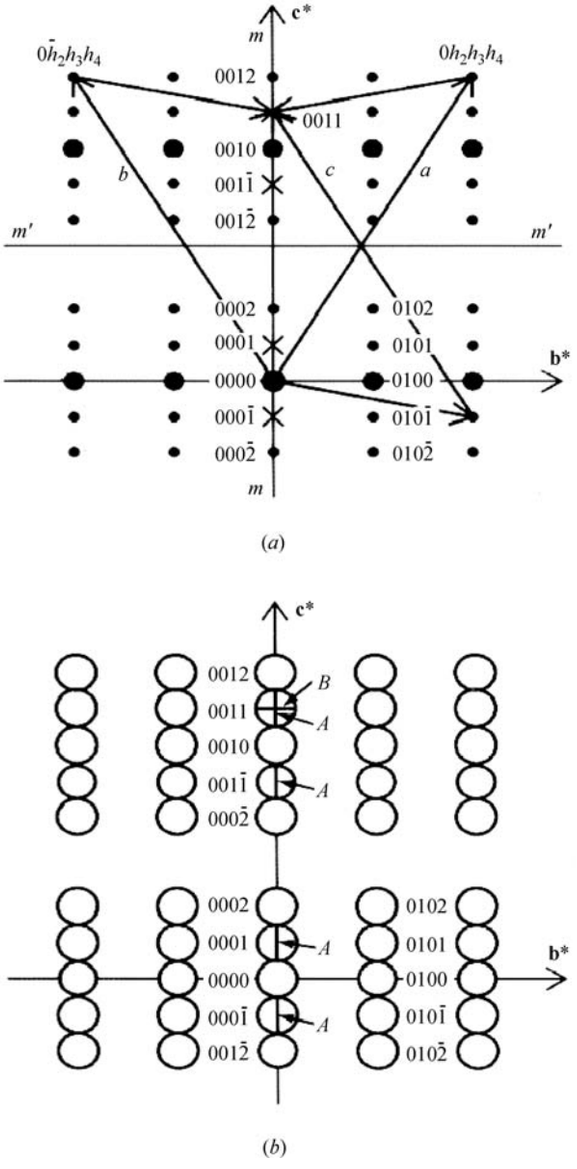

Fig. 2.5.3.21. (*a*) *Umweganregung* paths *a*, *b* and *c* to the 0011 forbidden reflection. (*b*) Expected dynamical extinction lines are shown, the 0011 reflection being excited. The wave number vector of modulation is $k_3\mathbf{c}^*$.

Thus, the following phase relations are obtained between the two structure factors:

$$\begin{aligned}
F(h_1h_2h_3h_4) &= F(h_1\bar{h}_2h_3h_4) \quad \text{for } h_4 \text{ even},\\
F(h_1h_2h_3h_4) &= -F(h_1\bar{h}_2h_3h_4) \quad \text{for } h_4 \text{ odd}.
\end{aligned} \tag{2.5.3.11}$$

These relations are analogous to the phase relations between the two structure factors for an ordinary three-dimensional crystal with a glide plane. The relations imply that dynamical extinction occurs for the glide planes and screw axes of the (3 + 1)-dimensional crystal with an infinite dimension along the direction of the incommensurate modulation wavevector **k**. Terauchi *et al.* (1994) showed that approximate dynamical extinction occurs for an incommensurate crystal of finite dimension.

Fig. 2.5.3.21(*a*) and (*b*) illustrate a spot diffraction pattern and a CBED pattern, respectively, expected from a modulated crystal with a (3 + 1)-dimensional space group $P^{P2mm}_{\bar{1}s\bar{1}}$ ($\mathbf{k} = k_3\mathbf{c}^*$) at the [100] incidence. The large and small spots in Fig. 2.5.3.21(*a*) designate the fundamental ($h_4 = 0$) and incommensurate reflections ($h_4 \neq 0$), respectively. The $00h_3h_4$ (h_4 = odd) reflections

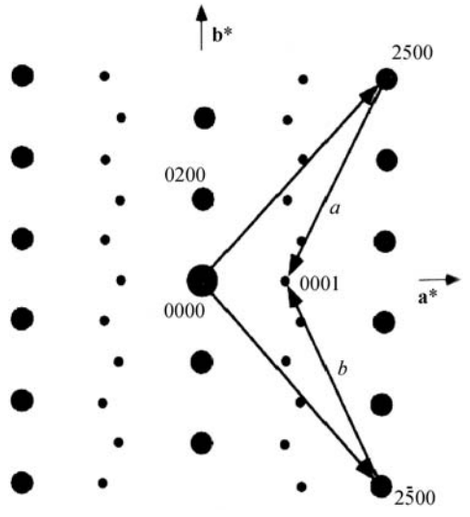

Fig. 2.5.3.22. Schematic diffraction pattern at the [001] incidence of $Sr_2Nb_2O_7$. *Umweganregung* paths *a* and *b via* fundamental reflections to the 0001 incommensurate reflection. Large and small spots denote fundamental and incommensurate reflections, respectively. The wave number vector of modulation is $\mathbf{k} = (\frac{1}{2} - \delta)\mathbf{a}^*$.

shown by crosses are kinematically forbidden by the glide plane (^m_s) perpendicular to the *b* axis. *Umweganregung* paths *a*, *b* and *c* in the ZOLZ to a kinematically forbidden reflection are drawn. The two paths *a* and *b* are geometrically equivalent with respect to the line *m*–*m* perpendicular to the *b* axis. Since every *Umweganregung* path to a kinematically forbidden reflection contains an odd number of $F(0h_{2,i}h_{3,i}h_{4,i})$ with odd $h_{4,i}$, the following equation is obtained.

$$F(0h_{2,1}h_{3,1}h_{4,1})F(0h_{2,2}h_{3,2}h_{4,2})\ldots F(0h_{2,n}h_{3,n}h_{4,n}) \quad \text{for path } a$$
$$= -F(0\bar{h}_{2,1}h_{3,1}h_{4,1})F(0\bar{h}_{2,2}h_{3,2}h_{4,2})\ldots F(0\bar{h}_{2,n}h_{3,n}h_{4,n})$$
$$\text{for path } b, \qquad (2.5.3.12)$$

where $\sum_{i=1}^{n} h_{2,i} = 0$, $\sum_{i=1}^{n} h_{3,i} = h_3$ and $\sum_{i=1}^{n} h_{4,i} = h_4$ (h_4 = odd).

When reflection $00h_3h_4$ (h_4 = odd) is exactly excited, the two paths *a* and *c* are symmetric with respect to the bisector m'–m' of the diffraction vector of the reflection and have the same excitation error. The waves passing through these paths have the same amplitude but different signs. Thus the following relation is obtained.

$$F(0h_{2,1}h_{3,1}h_{4,1})F(0h_{2,2}h_{3,2}h_{4,2})\ldots F(0h_{2,n}h_{3,n}h_{4,n}) \quad \text{for path } a$$
$$= -F(0\bar{h}_{2,n}h_{3,n}h_{4,n})F(0\bar{h}_{2,n-1}h_{3,n-1}h_{4,n-1})\ldots F(0\bar{h}_{2,1}h_{3,1}h_{4,1})$$
$$\text{for path } c, \qquad (2.5.3.13)$$

where $\sum_{i=1}^{n} h_{2,i} = 0$, $\sum_{i=1}^{n} h_{3,i} = h_3$ and $\sum_{i=1}^{n} h_{4,i} = h_4$ (h_4 = odd).

Therefore, dynamical extinction occurs in kinematically forbidden reflections of incommensurate crystals. Fig. 2.5.3.21(*b*) schematically shows the extinction lines in odd-order incommensurate reflections, where the 0011 reflection is exactly excited.

We consider the dynamical extinction from $Sr_2Nb_2O_7$ whose space group is $P^{Cmc2_1}_{\bar{1}\,s\,\bar{1}}$. The glide plane (^c_s) is perpendicular to the *b* axis with a glide vector $(\mathbf{c} + \mathbf{a}_4)/2$. The wave number vector of the modulation is $\mathbf{k} = (\frac{1}{2} - \delta)\mathbf{a}^*$. (Since space-group notation $Cmc2_1$ is broadly accepted, the direction of the modulation is taken as the *a* axis.) The reflections $h_10h_3h_4$ with $h_3 + h_4 = 2n + 1$ (n = integer) are kinematically forbidden. Fig. 2.5.3.22 shows a schematic diffraction pattern of $Sr_2Nb_2O_7$ at the [001] incidence. The large

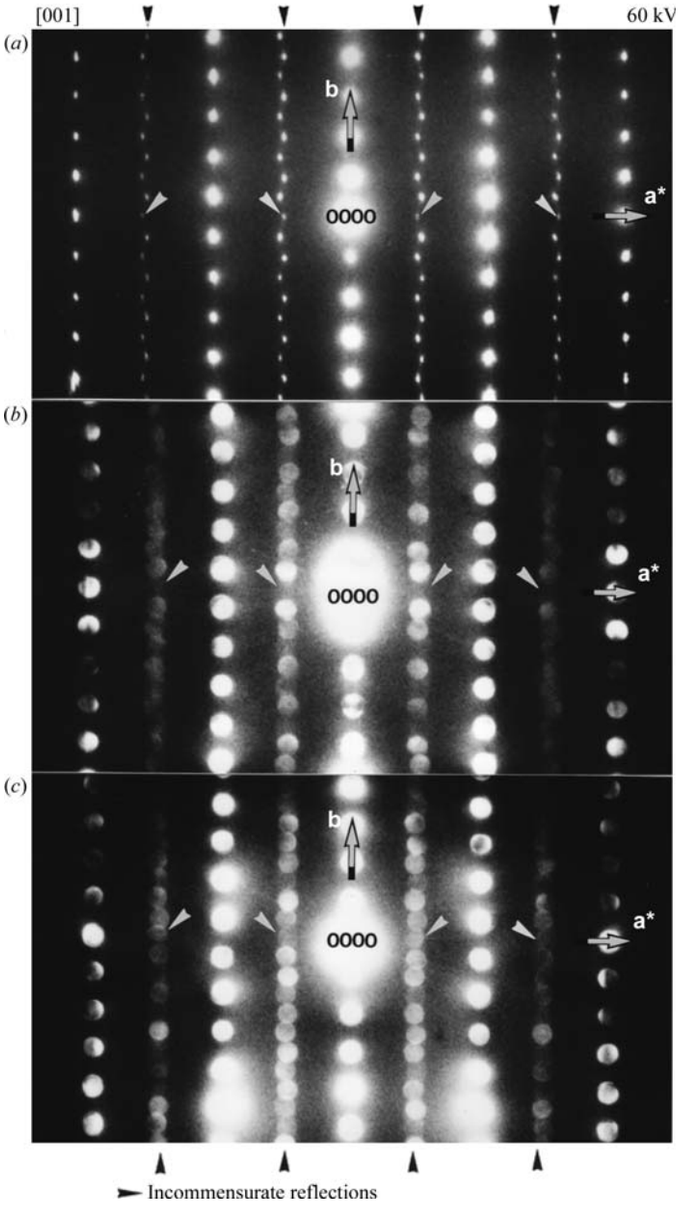

Fig. 2.5.3.23. Diffraction pattern of $Sr_2Nb_2O_7$ taken with [001] incidence at 60 kV. (*a*) Spot diffraction pattern. Kinematically forbidden 0001 and 200$\bar{1}$ incommensurate reflections exhibit definite intensity. (*b*) Zone-axis CBED pattern showing dynamical absence of 0001 and 200$\bar{1}$ incommensurate reflections. (*c*) CBED pattern taken at an incidence with a small tilt from the zone axis to the *b** direction. The kinematically forbidden incommensurate reflections have intensity due to incomplete cancellation of two waves through the *Umweganregung* paths. The wave number vector of modulation is $\mathbf{k} = (\frac{1}{2} - \delta)\mathbf{a}^*$.

and small spots indicate the fundamental (h_4 = 0) and incommensurate ($h_4 \neq 0$) reflections, respectively. *Umweganregung* paths *a* and *b* to the kinematically forbidden 0001 reflection *via* a fundamental reflection in the ZOLZ are drawn.

Fig. 2.5.3.23(*a*) shows a spot diffraction pattern of the incommensurate phase of $Sr_2Nb_2O_7$ taken with the [001] incidence at 60 kV. The incommensurate reflections in which dynamical extinction lines appear at this incidence are those with the indices $h_{1,\text{even}}00h_{4,\text{odd}}$ because $h_3 = 0$ and $h_1 + h_2 = 2n$ due to the lattice type *C* of the average structure.

The reflections in the four columns indicated by black arrowheads are incommensurate reflections. The reflections 0001, 000$\bar{1}$, 200$\bar{1}$ and $\bar{2}$001 designated by white arrowheads are kinematically forbidden but exhibit certain intensities, which are caused by multiple diffraction. Other reflections are fundamental reflections due to the average structure.

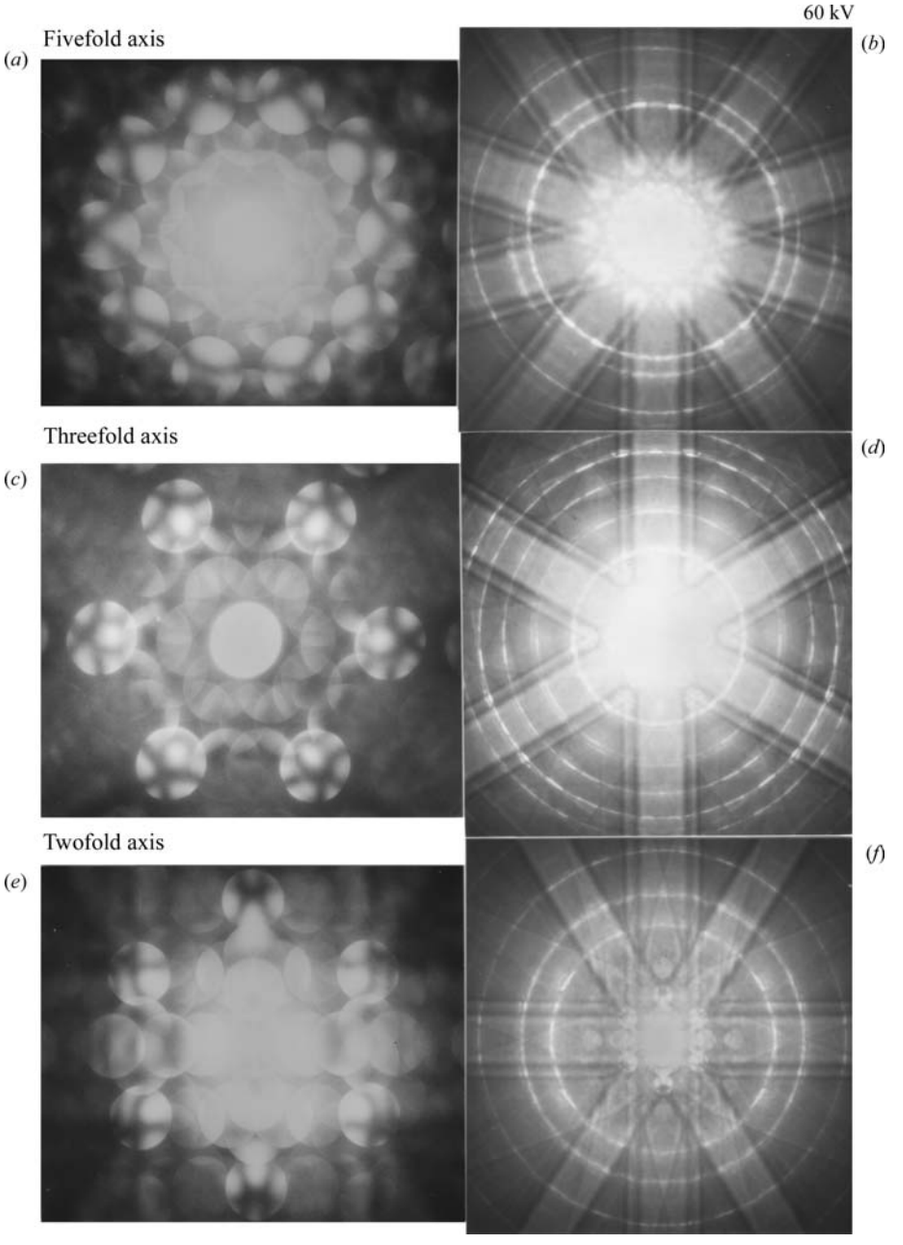

Fig. 2.5.3.24. Three pairs of ZOLZ [(*a*), (*c*) and (*e*)] and HOLZ [(*b*), (*d*) and (*f*)] CBED patterns taken at 60 kV from an area of $Al_{74}Mn_{20}Si_6$ about 3 nm in diameter and about 10 nm thick (Tanaka, Terauchi, Suzuki *et al.*, 1987). Symmetries are (*a*) 10*mm*, (*b*) 5*m*, (*c*) 6*mm*, (*d*) 3*m*, (*e*) 2*mm* and (*f*) 2*mm*.

Fig. 2.5.3.23(*b*) shows a CBED pattern corresponding to Fig. 2.5.3.23(*a*), taken from a specimen area 3 nm in diameter. The excitation errors of two *Umweganregung* paths *a* and *b* are the same at this electron incidence. The reflections 0001, $000\bar{1}$, $200\bar{1}$ and $\bar{2}001$ indicated by white arrowheads show no intensity. Dynamical extinction does not appear as a line in the present case because the width of the extinction line exceeds the disc size of the reflections. Fig. 2.5.3.23(*c*) shows a CBED pattern taken at an incidence slightly tilted toward the b^* axis from that for Fig. 2.5.3.23(*b*) or the [001] zone-axis incidence. The excitation errors are no longer the same for the two *Umweganregung* paths. Thus, it is seen that the kinematically forbidden reflections indicated by white arrowheads have intensities due to incomplete cancellation of waves coming through different paths, which is an additional proof of the dynamical extinction.

2.5.3.5. Symmetry determination of quasicrystals

2.5.3.5.1. Icosahedral quasicrystals

Penrose (1974) demonstrated that a two-dimensional plane can be tiled with thin and fat rhombi to give a pattern with local fivefold rotational symmetries but with no translational symmetry. Mackay (1982) extended the tiling to three dimensions using acute and obtuse rhombohedra, which also resulted in the acquisition of local fivefold rotational symmetries and in a lack of translational symmetry. The three-dimensional space-filling method was later completed by Ogawa (1985). These studies, however, remained a matter of design or geometrical amusement until Shechtman *et al.* (1984) discovered an icosahedral symmetry presumably with long-range structural order in an alloy of Al_6Mn (nominal composition) using electron diffraction. Since then, the term quasicrystalline order, a new class of structural order with no translational symmetry but long-range structural order, has been coined. Levine & Steinhardt (1984) showed that the quasilattice produces sharp diffraction patterns and succeeded in reproducing almost exactly the diffraction pattern obtained by Shechtman *et al*. (1984) using the Fourier transform of a quasi-periodic icosahedral lattice. When analysing X-ray and electron-diffraction data for a quasicrystal, the diffraction peaks can be successfully indexed by six independent vectors pointing to the vertices of an icosahedron. It was then found that the icosahedral quasicrystal can be described in terms of a regular crystal in six